Purkinje cell-specific males absent on the first (*mMof*) gene deletion results in an ataxia-telangiectasia-like neurological phenotype and backward walking in mice

Rakesh Kumar[a,b], Clayton R. Hunt[a,b], Arun Gupta[a,b], Suraj Nannepaga[c], Raj K. Pandita[b,d], Jerry W. Shay[d], Robert Bachoo[c], Thomas Ludwig[e], Dennis K. Burns[f], and Tej K. Pandita[a,b,1]

Departments of [a]Radiation Oncology, [c]Neurology, [d]Cell Biology, and [f]Pathology, University of Texas Southwestern Medical Center, Dallas, TX 75390; [b]Department of Radiation Oncology, Washington University School of Medicine, St. Louis, MO 63108; and [e]Institute for Cancer Genetics, Columbia University, New York, NY 10032

Edited* by Stephen P. Goff, Columbia University College of Physicians and Surgeons, New York, NY, and approved January 21, 2011 (received for review November 4, 2010)

The brains of ataxia telangiectasia (AT) patients display an aberrant loss of Purkinje cells (PCs) that is postulated to contribute to the observed deficits in motor coordination as well as in learning and cognitive function. AT patients have mutations in the ataxia telangiectasia mutated (*ATM*) gene [Savitsky et al. (1995) *Science* 268:1749–1753]. However, in *Atm*-deficient mice, the neurological defects are limited, and the PCs are not deformed or lost as observed in AT patients [Barlow et al. (1996) *Cell* 86:159–171]. Here we report that PC-specific deletion of the mouse males absent on the first (*mMof*) gene (*Cre*$^{-}$), which encodes a protein that specifically acetylates histone H4 at lysine 16 (H4K16ac) and influences ATM function, is critical for PC longevity. Mice deficient for PC-specific Mof display impaired motor coordination, ataxia, a backward-walking phenotype, and a reduced life span. Treatment of *Mof*$^{F/F}$*/Pcp2-Cre*$^{+}$ mice with histone deacetylase inhibitors modestly prolongs PC survival and delays death. Therefore, Mof expression and H4K16 acetylation are essential for PC survival and function, and their absence leads to PC loss and cerebellar dysfunction similar to that observed in AT patients.

ataxia telangiectasia phenotype | chromatin modification | DNA damage response

The most striking and obvious neurological manifestation seen in ataxia telangiectasia (AT) patients is a progressive cerebellar ataxia (1). Postmortem examination of brains from AT patients demonstrates significant loss and deformities in Purkinje cells (PCs) (2). Although a cause-and-effect relationship has not been proven, PC loss has a strong correlative association with AT. Mice deficient in ataxia telangiectasia mutated (Atm) display no gross ataxia or neuronal degeneration, but motor function is impaired without detectable PC deformity or loss (3, 4). Oxidative stress in PCs of $Atm^{-/-}$ mice is increased (5), probably resulting in increased DNA damage, the sensing and repair of which is ATM dependent (6–8). The mammalian males absent on the first (MOF) is an H4 histone acetylase that interacts with and influences downstream ATM functions in response to DNA damage (9). Through histone H4 acetylated at lysine 16 (H4K16ac), MOF has a critical role at multiple points in the cellular DNA damage response and repair of DNA double-strand breaks (10). Acetylation of histone H4 at K16 by MOF also is an epigenetic signature of cellular proliferation during both embryogenesis and oncogenesis (11), but whether MOF has a role in postmitotic cells is not known. In this study, we determined that MOF is required for postmitotic PC survival and that loss of MOF and H4K16 acetylation in PCs results in mice displaying neurological abnormalities similar to those encountered in AT patients.

Results and Discussion

Immunostaining of mouse cerebellum tissue sections confirmed endogenous MOF expression in PCs and the presence of acetylated H4K16 (Fig. S1). To deplete MOF specifically from PCs, mice containing a conditional floxed *mMof* gene ($Mof^{F/F}$) introduced by homologous recombination were crossed with mice expressing *Cre* recombinase from the PC-specific *Pcp2* gene promoter (12) to obtain $Mof^{F/F}$/*Pcp2-Cre*$^{-}$ and $Mof^{F/F}$/*Pcp2-Cre*$^{+}$ mice. The tissue-specific *Pcp2* promoter becomes maximally active 2–3 wk after birth, thus circumventing the embryonic-lethal effect of homozygous *mMof* deletion (11). In cerebellum collected from $Mof^{F/F}$/*Pcp2-Cre*$^{-}$ and $Mof^{F/F}$/*Pcp2-Cre*$^{+}$ mice at various times (10–65 d) after birth, MOF expression was easily detected in tissue from $Mof^{F/F}$/*Pcp2-Cre*$^{-}$ or $Mof^{F/F}$/*Pcp2-Cre*$^{+}$ mouse PCs at postnatal day 15, but expression was lost by postnatal day 25 in tissue from $Mof^{F/F}$/*Pcp2-Cre*$^{+}$ mice. As expected, MOF expression in PC-adjacent cell types was unaltered during the 65-d period examined (Fig. S2). Similarly, H4K16ac was easily detected in PCs from $Mof^{F/F}$/*Pcp2-Cre*$^{+}$ mice at postnatal day 15, but expression was gradually lost by postnatal day 35 (Fig. S2). Calbindin (a PC-specific cell marker) histochemical staining of cerebellum from age-matched $Mof^{F/F}$/*Pcp2-Cre*$^{-}$ and $Mof^{F/F}$/*Pcp2-Cre*$^{+}$ mice indicated that detectable PC loss in $Mof^{F/F}$/*Pcp2-Cre*$^{+}$ mice was first evident by postnatal day 25, increased to 40% of PCs by postnatal day 45, and finally reached 80% loss by postnatal day 65 (Fig. 1 and Figs. S3 and S4). A significant decrease ($P < 0.001$; Student's t test) in the number of PCs in $Mof^{F/F}$/*Pcp2-Cre*$^{+}$ mice was observed from about postnatal day 35 onwards, but there was no corresponding decrease in PC numbers in $Mof^{F/F}$/*Pcp2-Cre*$^{-}$ mouse brains (Fig. 1). Along with the loss of PC observed in brains $Mof^{F/F}$/*Pcp2-Cre*$^{+}$ mice, granular cells were visibly reduced (Fig. 1*A i* and *ii*). Numerous PCs in tissue from $Mof^{F/F}$/*Pcp2-Cre*$^{+}$ mice contained pyknotic nuclei, perhaps reflecting an altered chromatin state caused by decreasing H4K16ac (Fig. S2), a chromatin modification essential for protein–protein interactions (13). After the initial appearance of pyknotic-like PCs in tissue from $Mof^{F/F}$/*Pcp2-Cre*$^{+}$ mice, abnormal, coarse PC dendrites were detected with calbindin staining (Fig. 2 and Fig. S4).

The effect of PC-specific MOF loss on cerebellar cortical cytoarchitecture was analyzed further by H&E staining of cerebellum sections. No differences in the granular, PC or molecular layers were observed in tissue from 15-d-old $Mof^{F/F}$/*Pcp2-Cre*$^{+}$ or $Mof^{F/F}$/*Pcp2-Cre*$^{-}$ mice. However, by postnatal day 25, occasional

Author contributions: R.K., R.B., T.L., D.K.B., and T.K.P. designed research; R.K., A.G., S.N., R.K.P., and T.L. performed research; T.L. and D.K.B. contributed new reagents/analytic tools; R.K., C.R.H., J.W.S., R.B., D.K.B., and T.K.P. analyzed data; and C.R.H., J.W.S., D.K.B., and T.K.P. wrote the paper.

The authors declare no conflict of interest.

*This Direct Submission article had a prearranged editor.

[1]To whom correspondence should be addressed. E-mail: tej.pandita@utsouthwestern.edu.

This article contains supporting information online at www.pnas.org/lookup/suppl/doi:10.1073/pnas.1016524108/-/DCSupplemental.

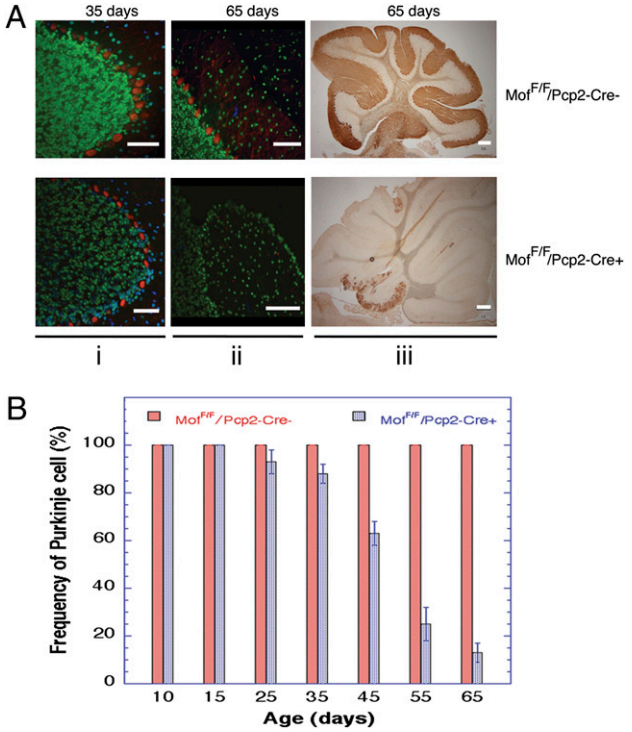

Fig. 1. PCs in cerebellum of *Mof*$^{F/F}$/*Pcp2-Cre*$^{-}$ and *Mof*$^{F/F}$/*Pcp2-Cre*$^{+}$ mice. (*A*) Calbindin staining of cerebellum. (*i* and *ii*) Immunofluorescence staining for calbindin (red) and H4k16ac (green) of ventricle IV from cerebellum of *Mof*$^{F/F}$/*Pcp2-Cre*$^{-}$ and *Mof*$^{F/F}$/*Pcp2-Cre*$^{+}$ mice at postnatal days 35 (*i*) and 65 (*ii*). Loss of PCs is quite prominent in 65-d-old *Mof*$^{F/F}$/*Pcp2-Cre*$^{+}$ mice. (*iii*) PC identification by calbindin detection by HRP staining. Cerebellums of 65-d-old *Mof*$^{F/F}$/*Pcp2-Cre*$^{+}$ mice show widespread loss of PCs and PC dendritic calbindin activity with some residual PC in the 10th lobe. (*B*) PC density at various ages, demonstrating progressive PC loss in *Mof*$^{F/F}$/*Pcp2-Cre*$^{+}$ mice.

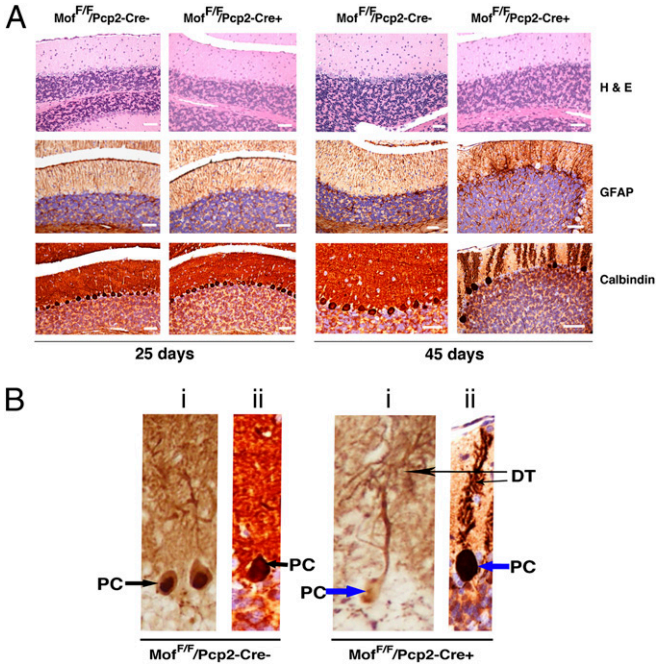

Fig. 2. Histologically stained sagittal sections of cerebellum from *Mof*$^{F/F}$/*Pcp2-Cre*$^{+}$ and *Mof*$^{F/F}$/*Pcp2-Cre*$^{-}$ mice. (*A*) (*Top*) H&E staining reveals minimal pyknotic PCs in 25-d-old *Mof*$^{F/F}$/*Pcp2-Cre*$^{+}$ mice, but by postnatal day 45 the frequency of degenerating PCs with pyknotic nuclei and eosinophilic cytoplasm increases substantially. (*Middle*) GFAP staining reveals that levels are similar in cerebellum of 25-d-old *Mof*$^{F/F}$/*Pcp2-Cre*$^{+}$ and *Mof*$^{F/F}$/*Pcp2-Cre*$^{+}$ mice; however, GFAP levels are increased only in cerebellum of 45-d-old *Mof*$^{F/F}$/*Pcp2-Cre*$^{+}$ mice, most conspicuously in areas of PC loss. (*Bottom*) Calbindin staining shows similar frequency of PC cells in cerebellum of 25-d-old *Mof*$^{F/F}$/*Pcp2-Cre*$^{+}$ and *Mof*$^{F/F}$/*Pcp2-Cre*$^{+}$ mice; however, PC degeneration along with dendrite loss is quite visible in cerebellum of 45-d-old *Mof*$^{F/F}$/*Pcp2-Cre*$^{+}$ mice. (*B*) Comparison of calbindin-stained PC from *Mof*$^{F/F}$/*Pcp2-Cre*$^{-}$ mice (*Left*) and *Mof*$^{F/F}$/*Pcp2-Cre*$^{+}$ mice (*Right*) at higher magnification. DT, dendrite. (*i*) Twenty-five days. (*ii*) Forty-five days.

pyknotic PC nuclei became apparent in tissue from *Mof*$^{F/F}$/*Pcp2-Cre*$^{+}$ mice (Fig. 2 and Fig. S5). Most strikingly, by postnatal day 45 there was a substantial increase in the numbers of pyknotic PCs and degenerating PCs, accompanied by areas of frank PC loss and modestly increased numbers of Bergmann glia at the granule cell–molecular layer interface in tissue from *Mof*$^{F/F}$/*Pcp2-Cre*$^{+}$ mice (Fig. 2 and Figs. S6 and S7).

Cerebellum GFAP is necessary for the integrity of central nervous system white-matter architecture and long-term maintenance of myelination (14). GFAP levels in immunostained sections of cerebellum from 15-d-old *Mof*$^{F/F}$/*Pcp2-Cre*$^{+}$ and *Mof*$^{F/F}$/*Pcp2-Cre*$^{-}$ mice were similar. However, at postnatal day 25 the intensity of GFAP staining was higher in tissue from *Mof*$^{F/F}$/*Pcp2-Cre*$^{+}$ mice than in tissue from *Mof*$^{F/F}$/*Pcp2-Cre*$^{-}$ mice (Fig. 2 and Fig. S8), and this intensity increased further by day 45 (Fig. 2 and Fig. S9). The increased GFAP expression observed is compatible with the Bergmann gliosis noted in areas of PC loss.

PCs send inhibitory projections to the deep cerebellar and vestibular nuclei, which are the only source of output from the cerebellar cortex (15). The most obvious clinical manifestation seen in AT patients is progressive cerebellar ataxia (1) attributable to the profound loss of PCs seen in postmortem brains (2). Therefore, we investigated whether MOF depletion in mouse PCs results in abnormal motor coordination. We observed that, beginning around postnatal day 35, *Mof*$^{F/F}$/*Pcp2-Cre*$^{+}$ mice are much less active than *Mof*$^{F/F}$/*Pcp2-Cre*$^{-}$ mice (Movie S1) and display very slow forward walking (Movie S2). More interestingly, by postnatal day 45 more than 65% of *Mof*$^{F/F}$/*Pcp2-Cre*$^{+}$ mice display the curious phenotype of backward walking (Fig. 3*A* and Movie S2), and there is a direct correlation between the progression of PC loss and initiation of backward walking. By postnatal day 55, *Mof*$^{F/F}$/*Pcp2-Cre*$^{+}$ mice exhibit only backward walking in open field until they die (Fig. 4*A* and Movies S3 and S4). A prominent visible ataxia of rapid head shaking was observed only in *Mof*$^{F/F}$/*Pcp2-Cre*$^{+}$ mice after postnatal day 45 (Movie S5), a phenotype that has not been observed in *Atm*-null mice (3, 4).

Results from sensorimotor testing indicated that *Mof*$^{F/F}$/*Pcp2-Cre*$^{+}$ mice were impaired on the elevated platform test relative to *Mof*$^{F/F}$/*Pcp2-Cre*$^{-}$ controls (Fig. 3*B*), as evidenced by the *Mof*$^{F/F}$/*Pcp2-Cre*$^{+}$ mice spending significantly less time on the platform [$F(1,12) = 10.48$; $P = 0.007$]. However, the groups did not differ in other measures within the battery (e.g., ledge, pole, or 90° inclined or inverted screen), suggesting that the impaired performance on the platform test represented a relatively specific deficit, possibly involving disturbed balance. These tests were performed at the age of 6–9 wk, when >40% of PCs were lost in *Mof*$^{F/F}$/*Pcp2-Cre*$^{+}$ mice.

Rotarod testing indicated that the *Mof*$^{F/F}$/*Pcp2-Cre*$^{+}$ mice also were impaired on tasks that required fine-motor coordination, with deficits becoming more apparent with increasing task difficulty. For example, the *Mof*$^{F/F}$/*Pcp2-Cre*$^{+}$ mice exhibited mild performance deficits in their ability to remain on the stationary rod (Fig. 3*C*) [main effect of Genotype (PC-specific mMof knockout in mice vs. control): $F(1,12) = 5.21$; $P = 0.042$], whereas their performance on the constant speed and acceler-

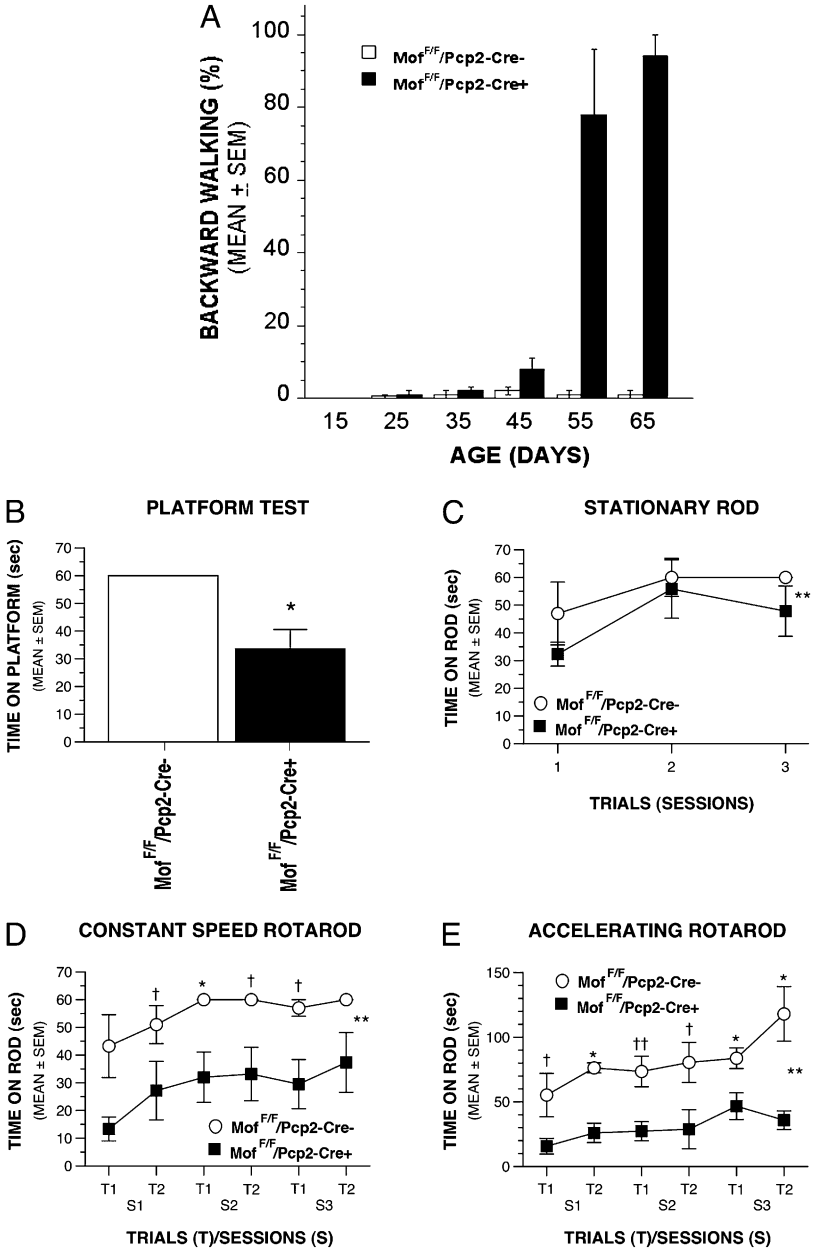

Fig. 3. Behavioral studies of *Mof*$^{F/F}$/*Pcp2-Cre*$^{-}$ and *Mof*$^{F/F}$/*Pcp2-Cre*$^{+}$ mice. (*A*) *Mof*$^{F/F}$/*Pcp2-Cre*$^{+}$ mice showed prominent backward walking as shown in SI movies. Significant backward walking of *Mof*$^{F/F}$/*Pcp2-Cre*$^{+}$ mice was observed after postnatal day 45. (*B*) Results from the elevated platform test showed that *Mof*$^{F/F}$/*Pcp2-Cre*$^{+}$ mice were able to remain on a small, circular, elevated platform for a significantly shorter time than *Mof*$^{F/F}$/*Pcp2-Cre*$^{-}$ mice (*$P = 0.007$), suggesting impaired balance in *Mof*$^{F/F}$/*Pcp2-Cre*$^{+}$ mice. (*C*–*E*) Results from the Rotarod test suggest that the *Mof*$^{F/F}$/*Pcp2-Cre*$^{+}$ mice had mild balance deficits and severe impairments in fine-motor coordination. (*C*) On average across the test sessions, *Mof*$^{F/F}$/*Pcp2-Cre*$^{+}$ mice spent significantly less time than *Mof*$^{F/F}$/*Pcp2-Cre*$^{-}$ mice on the stationary rod of the Rotarod test (**$P = 0.042$). (*D*) On the constant-speed Rotarod, *Mof*$^{F/F}$/*Pcp2-Cre*$^{+}$ mice spent a significantly shorter amount of time than *Mof*$^{F/F}$/*Pcp2-Cre*$^{-}$ mice on the rotating rod (**$P = 0.005$) across the test sessions. Differences were significantly different between groups for session 2 of trial 1 (*$P = 0.008$), and large differences also were observed for session 1 of trial 2, session 2 of trial 2, and session 3 of trial 1 ($^{\dagger}P < 0.049$). (*E*) *Mof*$^{F/F}$/*Pcp2-Cre*$^{+}$ mice spent a significantly shorter period than *Mof*$^{F/F}$/*Pcp2-Cre*$^{-}$ mice on the accelerating rotating rod (**$P = 0.0005$) across the test sessions. Pairwise comparisons showed significant differences between groups in session 1 of trial 2, and in session 3 of both trials (*$P < 0.003$); large differences also were also observed in session 2 of trial 1 ($^{\dagger\dagger}P = 0.009$) and in the other remaining trials ($^{\dagger}P < 0.035$).

ating Rotarod components was impaired (Fig. 3 *D* and *E*). Specifically, an analysis of the constant speed Rotarod data revealed that, on average across test sessions, the *Mof*$^{F/F}$/*Pcp2-Cre*$^{+}$ mice remained on the rotating rod for a significantly shorter time than the *Mof*$^{F/F}$/*Pcp2-Cre*$^{-}$ mice, although performance generally improved across test sessions [significant effects of Genotype, $F(1,12) = 11.98$, $P = 0.005$, and Test Session, $F(2,24) = 4.73$, $P = 0.022$]. Even greater performance impairments were observed in the ability of *Mof*$^{F/F}$/*Pcp2-Cre*$^{+}$ mice to stay on the accelerating Rotarod [significant effects of Genotype, $F(1,12) = 22.63$, $P = 0.0005$, and Test Session, $F(2,24) = 11.60$, $P = 0.0003$]. In summary, the Rotarod data suggest that *Mof*$^{F/F}$/*Pcp2-Cre*$^{+}$ mice are impaired on tasks requiring fine-motor coordination (constant speed Rotarod and accelerating Rotarod tests) (Fig. 3 *D* and *E*). These behavioral analyses indicate that *Mof*$^{F/F}$/*Pcp2-Cre*$^{+}$ mice have a behavioral phenotype of severe

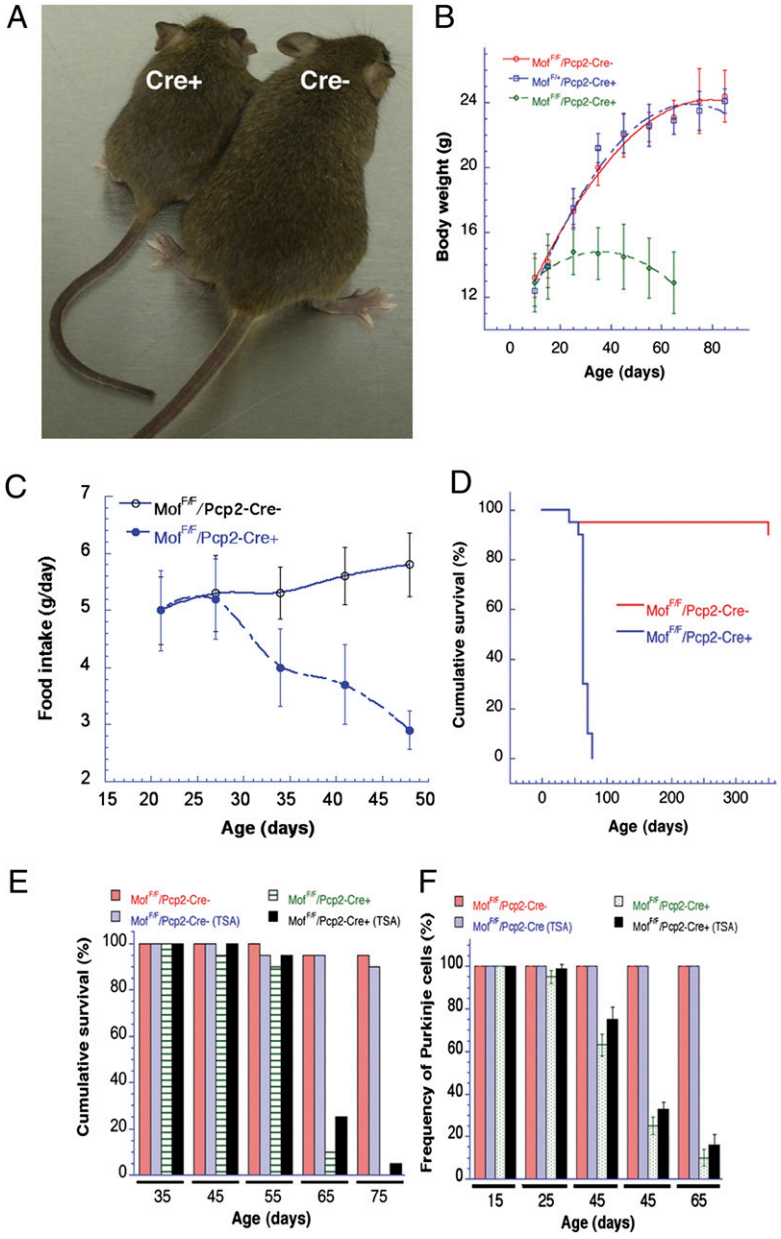

Fig. 4. Effect of MOF and HDACi treatment on body weight, survival, and PC numbers. (*A*) *Mof*$^{F/F}$*/Pcp2-Cre*$^{+}$ (*Left*) and *Mof*$^{F/F}$*/Pcp2*-Cre^{-} (*Right*) mice at postnatal day 45. (*B*) Body weight of *Mof*$^{F/F}$*/Pcp2-Cre*$^{+}$ mice decreased after postnatal day 30. (*C*) Comparison of food intake by *Mof*$^{F/F}$*/Pcp2-Cre*$^{+}$ and *Mof*$^{F/F}$*/Pcp2-Cre*$^{-}$ mice. (*D*) Survival of *Mof*$^{F/F}$*/Pcp2-Cre*$^{+}$ mice was significantly decreased relative to *Mof*$^{F/+}$*/Pcp2-Cre*$^{-}$ mice. Mice with PC-specific knockout of the *mMof* gene (*Mof*$^{F/F}$*/Pcp2-Cre*$^{+}$) die at 61 ± 12 d after birth, whereas *Mof*$^{F/F}$*/Pcp2-Cre*$^{-}$ mice remain healthy. (*E*) TSA has a positive effect on the cumulative survival of *Mof*$^{F/F}$*/Pcp2-Cre*$^{+}$ mice but not *Mof*$^{F/F}$*/Pcp2-Cre*$^{-}$ mice. (*F*) TSA affects the frequency of PCs in *Mof*$^{F/F}$*/Pcp2-Cre*$^{+}$ mice but not in *Mof*$^{F/F}$*/Pcp2-Cre*$^{-}$ mice.

impairment in fine-motor coordination and possibly mild balance disturbances. These results are consistent with previous findings using the same tests to characterize functional deficits in other strains of mutant mice that have synaptic defects in cerebellar PCs (16), mice that have nonreceptor Abl/Arg tyrosine kinase-related cerebellum defects (17), and Atm-deficient mice (3).

The physiological effect of PC loss induced by MOF depletion was readily visible (Fig. 4). Although the total body weight of *Mof*$^{F/F}$*/Pcp2-Cre*$^{+}$ and *Mof*$^{F/F}$*/Pcp2-Cre*$^{-}$ mice was similar at postnatal day 15, the growth of *Mof*$^{F/F}$*/Pcp2-Cre*$^{+}$ mice was significantly reduced subsequently, with maximal total body weight reached 25–45 d after birth that was <50% of the weight of age-matched *Mof*$^{F/F}$*/Pcp2-Cre*$^{-}$ mice. After age 45 d, the body weight of *Mof*$^{F/F}$*/Pcp2-Cre*$^{+}$ mice began to decline (Fig. 4 *A* and *B*). The loss of body weight in *Mof*$^{F/F}$*/Pcp2-Cre*$^{+}$ mice correlated with a decrease in food intake compared with *Mof*$^{F/F}$*/Pcp2-Cre*$^{-}$ mice (Fig. 4*C*). Overall survival was dramatically decreased in *Mof*$^{F/F}$*/Pcp2-Cre*$^{+}$ mice, with the majority dying within 55–65 d after birth and none surviving longer than 75 d (Fig. 4*D*).

The H4K16ac modification poses a structural constraint on the formation of higher-order chromatin (13), perhaps inducing an open chromatin configuration that is more readily accessible to transcription as well as DNA repair. Acetylation of histone H4 at K16 also is critical for protein–protein interactions (18), and the only mammalian protein known to perform this function is MOF (9, 10, 19, 20), Recently, we reported that cells treated with trichostatin A (TSA) had increased levels of H4K16ac but unaltered MOF protein levels (10). We therefore investigated

whether inhibition of H4K16ac de-acetylation with two different histone deacetylase inhibitors (HDACi), TSA and EX-527 (21), would improve survival by delaying PC loss in *Mof*$^{F/F}$/*Pcp2-Cre*$^{+}$ mice. Short-term drug treatment of *Mof*$^{F/F}$/*Pcp2-Cre*$^{+}$ mice initiated 30–35 d after birth delayed mouse death (Fig. 4*E*). A further delay in initiating treatment to postnatal day 55 failed to extend lifespan (Fig. 4 and Fig. S10). If drug treatment began at postnatal day 35, a slight, but still significant, increase in PC survival was observed in *Mof*$^{F/F}$/*Pcp2-Cre*$^{+}$ mice, and such mice also had a 10–12% increase in lifespan.

There was no difference in the number of PCs in *Mof*$^{F/F}$/*Pcp2-Cre*$^{+}$ or *Mof*$^{F/F}$/*Pcp2-Cre*$^{-}$ mice after treatment with TSA during postnatal days 10–15. This lack of effect probably reflects the period before cellular MOF levels began decreasing because of Cre recombinase expression. However, when mice were treated with TSA beginning on postnatal day 20, PC loss was significantly delayed in *Mof*$^{F/F}$/*Pcp2-Cre*$^{+}$ mice as compared with *Mof*$^{F/F}$/*Pcp2-Cre*$^{-}$ mice (Fig. 4*F*). The delay in loss of PCs in *Mof*$^{F/F}$/*Pcp2-Cre*$^{+}$ mice was most prominent when mice were treated during postnatal days 25–45. However, TSA had a minimal effect on *Mof*$^{F/F}$/*Pcp2-Cre*$^{+}$ mice when treatment was initiated at postnatal day 45. We tested another HDACi, EX-527, which also is known to increase H4K16ac levels (21, 22). *Mof*$^{F/F}$/*Pcp2-Cre*$^{+}$ mice administered EX-527 also displayed a delay in PC loss (Fig. S10). HDACi treatment in *Mof*$^{F/F}$/*Pcp2-Cre*$^{+}$ mice not only delayed the loss of PCs in *Mof*$^{F/F}$/*Pcp2-Cre*$^{+}$ mice but also increased lifespan by about 12% (Fig. 4 and Fig. S10). Because in vitro treatment with TSA as well as EX-527 is known to increase H4K16ac levels (10, 21, 22), the present studies support the argument that H4K16ac has a critical role in maintaining PC functions.

We report here that PC-specific deletion of the *Mof* gene in mice produces neurological abnormalities attributable to cerebellar dysfunction that are similar to those seen in AT patients, including impaired fine-motor coordination, balance deficits, ataxia, and a most unusual backward-walking phenotype. Examination of the corresponding mouse cerebellum indicates PC depletion, which is also observed postmortem in AT patient brains. Taken together, these results suggest that the PC-specific Mof-deletion mouse mimics the physiological developments seen in AT patients. MOF also interacts with and influences downstream ATM functions in response to DNA damage (9, 10, 23), suggesting defective communication along the MOF/ATM pathway in PCs. Analysis of this pathway under conditions of oxidative stress, as occurs in the absence of ATM, may offer explanations as to the development of other AT-related symptoms. In addition, these mice provide a valuable means for understanding the role of chromatin-modifying factors, such as MOF, in the function and survival of nonproliferating postmitotic cells, especially neuronal cells. Further advances will require the development of specific deacetylation inhibitors, such as ones targeting the MOF modification product histone H4K16ac, which could facilitate future treatment possibilities.

Materials and Methods

Generation of PC-Specific *mMof*-Deficient Mice. Targeting vectors for the *mMof* locus were constructed to generate an in vivo deletion of the *mMof* gene in mice. The details of generating a conditional *mMof* allele by inserting a single *loxP* site together with a flippase recombination target (FRT)-flanked hygromycin resistance gene cassette 1.5 kb upstream of the *mMof* transcription initiation site and a second *loxP* site within intron 3 were described recently (11). The construct was electroporated into W9.5 ES cells to generate *Mof*$^{flox/+}$ cells. Details for generation of *Mof*$^{flox/+}$/*Rosa26*$^{creERT2/+}$ and *Mof* $^{Dflox/flox}$/*Rosa26*$^{creERT2/+}$ ES cell clones have been described (11).

To generate Purkinje cell-specific Mof-deficient mice using the Cre/loxP recombination system, Mof$^{flox/flox}$ mice, which contained two *loxP* sites flanking exon 3 of the *Mof* gene, were crossed with pcp2-*Cre* transgenic mice [B6.129-Tg(Pcp2-cre)2Mpin/J] (Jackson Laboratory) expressing Cre recombinase under the control of a L7/Pcp2 promoter (24). All procedures relating to the care and treatment of the animals were performed in accordance with the National Institutes of Health guidelines at Washington University School of Medicine, St. Louis, Columbia University, New York, and University of Texas Southwestern Medical Center, Dallas.

PCR Analysis of Genomic DNA. Genomic DNA was prepared from mouse tail and several brain regions, including the olfactory bulb, cortex, and cerebellum, using the HotSHOT method (25). PCR was performed using a RoboCycler (Stratagene) with Taq DNA polymerase (QiaTaq; Qiagen). The procedures for primer selection and conditions used for PCR genotyping were as described previously (11).

Histology and Immunohistochemistry. We analyzed the status of cerebellum PCs using fresh-frozen sections as well as paraffin-embedded sections. Mice were perfused with 4% paraformaldehyde, and dissected brains were perfusion-fixed for 36 h before paraffin embedding.

Fixation and Sectioning. After harvest, mouse brains were removed and perfusion-fixed with 4% paraformaldehyde. After fixation, hindbrains (brainstem and cerebellum) were divided into four sections in the sagittal plane. Tissues were dehydrated in xylene, embedded in paraffin, and sectioned on a rotary microtome at 3-mm thicknesses. For routine histology, paraffin sections were rehydrated, stained with H&E, and evaluated by light microscopy.

Immunohistochemistry. Immunostaining was performed at room temperature on a BenchMarkXT automated immunostainer, using the UltraVIEW system with HRP and diaminobenzidine (DAB) chromogen (Ventana Medical Systems). Optimum primary antibody dilutions were predetermined using known positive-control tissues. Paraffin sections were cut at 3 μm on a rotary microtome, mounted on positively charged glass slides, and air-dried overnight. Sections then were placed onto the BenchMarkXT where the deparaffinization and heat retrieval were performed. Sections then were incubated for 1 h with primary mouse monoclonal antibody to calbindin (1:50 dilution; Novocastra/Leica) or rabbit polyclonal antibody to glial fibrillary acidic protein (1:400 dilution; Biocare) diluted in ChemMate buffer (Ventana Medical Systems) or with buffer alone as a negative reagent control. After washing in buffer, sections were incubated with a freshly prepared mixture of DAB and H_2O_2 in buffer for 8 min, followed by washing in buffer and then in water. Sections were counterstained with hematoxylin, dehydrated in a graded series of ethanols and xylene, and coverslipped. Slides were reviewed by light microscopy. Positive reactions with DAB were identified as dark brown reaction product.

PC Counting. The number of PCs was quantified in midsagittal, 100-mm-thick cerebellar sections prepared from age-matched *Mof*$^{F/F}$/Pcp2-*Cre*$^{-}$ and *Mof* $^{F/F}$/*Pcp2-Cre*$^{+}$ mice at different ages (n = 4 for each age group). Optical images of PCs immunostained with anti-calbindin antibody were taken using 2×, 10×, and 20× objective lenses.

Reagents. TSA purchased from Sigma was dissolved in DMSO and administered in vivo at 1 mg·kg of body weight^{-1}·d^{-1} for 10 d. EX527 was purchased from Tocris and dissolved in 4% DMSO/10% cyclodextrin in PBS and administered in vivo at 1 mg·kg of body weight^{-1}·d^{-1} for 10 d.

Quantitation of Food Intake. Standard procedures (26) for quantitating mouse food intake were used. In brief, mice were acclimatized to individual cages for 1 wk. Food intake was measured every week. The body weight of individual mice was measured before and after each test series. Chow intake was measured by weighing the cage tops containing food pellets. Cage bottoms were covered with polyvinyl sheets when the cage tops were weighed, and any food spilled on sheets was collected and weighed. Food intake was corrected for spillage.

Behavioral Studies. To provide an initial characterization of the functional deficits in *Mof*$^{F/F}$/*Pcp2-Cre*$^{+}$ mice, they and littermate *Mof*$^{F/F}$/*Pcp2-Cre*$^{-}$ controls were evaluated on a battery of sensorimotor measures and the Rotarod test at 6–9 wk of age. These behavioral analyses have been used previously to assess ataxias, including ataxias of cerebellar origin, in several different mutant mouse strains (16, 27, 28), and these methodologies are described briefly in *SI Materials and Methods*. All behavioral tests were conducted by individuals who were unaware of the genotypic status of the mice (*SI Materials and Methods*).

ACKNOWLEDGMENTS. We thank David Woznaik, Sara Converys, Peter McKinnon, Mark Goldberg, and Ann Stowe for help with animal behavior studies, suggestions, and comments. We thank members of the T.K.P. laboratory for helpful discussions and suggestions. We also thank Swati Pandita for editing movies and graphic work. This work was supported by National Institutes of Health/National Cancer Institute Grants R01CA123232, R01CA129537, RO1CA154320, and R13CA130756.

1. Sedgwick RP, Boder E (1960) Progressive ataxia in childhood with particular reference to ataxia-telangiectasia. *Neurology* 10:705–715.
2. Boder E, Sedgwick RP (1958) Ataxia-telangiectasia; a familial syndrome of progressive cerebellar ataxia, oculocutaneous telangiectasia and frequent pulmonary infection. *Pediatrics* 21:526–554.
3. Barlow C, et al. (1996) Atm-deficient mice: A paradigm of ataxia telangiectasia. *Cell* 86:159–171.
4. Barlow C, et al. (2000) ATM is a cytoplasmic protein in mouse brain required to prevent lysosomal accumulation. *Proc Natl Acad Sci USA* 97:871–876.
5. Huang C, Sloan EA, Boerkoel CF (2003) Chromatin remodeling and human disease. *Curr Opin Genet Dev* 13:246–252.
6. Lavin MF (2008) Ataxia-telangiectasia: From a rare disorder to a paradigm for cell signalling and cancer. *Nat Rev Mol Cell Biol* 9:759–769.
7. Pandita TK, Richardson C (2009) Chromatin remodeling finds its place in the DNA double-strand break response. *Nucleic Acids Res* 37:1363–1377.
8. Pandita TK (2003) A multifaceted role for ATM in genome maintenance. *Expert Rev Mol Med* 5:1–21.
9. Gupta A, et al. (2005) Involvement of human MOF in ATM function. *Mol Cell Biol* 25: 5292–5305.
10. Sharma GG, et al. (2010) MOF and histone H4 acetylation at lysine 16 are critical for DNA damage response and double-strand break repair. *Mol Cell Biol* 30:3582–3595.
11. Gupta A, et al. (2008) The mammalian ortholog of Drosophila MOF that acetylates histone H4 lysine 16 is essential for embryogenesis and oncogenesis. *Mol Cell Biol* 28: 397–409.
12. Zhang XM, et al. (2004) Highly restricted expression of Cre recombinase in cerebellar Purkinje cells. *Genesis* 40:45–51.
13. Shogren-Knaak M, et al. (2006) Histone H4-K16 acetylation controls chromatin structure and protein interactions. *Science* 311:844–847.
14. Gerbert J, Burns S, Liedtke LA (1996) Anesthesia blocks of the lower extremity. Comparing the Biojector with needle and syringe. *J Am Podiatr Med Assoc* 86: 195–204.
15. Ito M, Yoshida M, Obata K, Kawai N, Udo M (1970) Inhibitory control of intracerebellar nuclei by the Purkinje cell axons. *Exp Brain Res* 10:64–80.
16. Grady RM, Wozniak DF, Ohlemiller KK, Sanes JR (2006) Cerebellar synaptic defects and abnormal motor behavior in mice lacking alpha- and beta-dystrobrevin. *J Neurosci* 26:2841–2851.
17. Qiu Z, Cang Y, Goff SP (2010) Abl family tyrosine kinases are essential for basement membrane integrity and cortical lamination in the cerebellum. *J Neurosci* 30: 14430–14439.
18. Neal KC, Pannuti A, Smith ER, Lucchesi JC (2000) A new human member of the MYST family of histone acetyl transferases with high sequence similarity to Drosophila MOF. *Biochim Biophys Acta* 1490:170–174.
19. Smith ER, et al. (2005) A human protein complex homologous to the Drosophila MSL complex is responsible for the majority of histone H4 acetylation at lysine 16. *Mol Cell Biol* 25:9175–9188.
20. Taipale M, et al. (2005) hMOF histone acetyltransferase is required for histone H4 lysine 16 acetylation in mammalian cells. *Mol Cell Biol* 25:6798–6810.
21. Solomon JM, et al. (2006) Inhibition of SIRT1 catalytic activity increases p53 acetylation but does not alter cell survival following DNA damage. *Mol Cell Biol* 26: 28–38.
22. Hajji N, et al. (2010) Opposing effects of hMOF and SIRT1 on H4K16 acetylation and the sensitivity to the topoisomerase II inhibitor etoposide. *Oncogene* 29:2192–2204.
23. Li X, et al. (2010) MOF and H4 K16 acetylation play important roles in DNA damage repair by modulating recruitment of DNA damage repair protein Mdc1. *Mol Cell Biol* 30:5335–5347.
24. Barski JJ, Dethleffsen K, Meyer M (2000) Cre recombinase expression in cerebellar Purkinje cells. *Genesis* 28:93–98.
25. Truett GE, et al. (2000) Preparation of PCR-quality mouse genomic DNA with hot sodium hydroxide and Tris (HotSHOT). *Biotechniques* 29:52, 54.
26. Bachmanov AA, Reed DR, Tordoff MG, Price RA, Beauchamp GK (2001) Nutrient preference and diet-induced adiposity in C57BL/6ByJ and 129P3/J mice. *Physiol Behav* 72:603–613.
27. Wang Q, et al. (2002) Ataxia and paroxysmal dyskinesia in mice lacking axonally transported FGF14. *Neuron* 35:25–38.
28. Griffey MA, et al. (2006) CNS-directed AAV2-mediated gene therapy ameliorates functional deficits in a murine model of infantile neuronal ceroid lipofuscinosis. *Mol Ther* 13:538–547.